STROKENET: A NEURAL PAINTING ENVIRONMENT

Anonymous authors
Paper under double-blind review

ABSTRACT

We've seen tremendous success of image generating models these years. Generating images through a neural network is usually pixel-based, which is fundamentally different from how humans create artwork using brushes. To imitate human drawing, interactions between the environment and the agent is required to allow trials. However, the environment is usually non-differentiable, leading to slow convergence and massive computation. In this paper we try to address the discrete nature of software environment with an intermediate, differentiable simulation. We present **StrokeNet**, a novel model where the agent is trained upon a well-crafted neural approximation of the painting environment. With this approach, our agent was able to learn to write characters such as MNIST digits very quickly in an unsupervised manner. Our primary contribution is the neural simulation of a real-world environment. Furthermore, the agent trained with the emulated environment is able to directly transfer its skills to real-world software. [1]

1 INTRODUCTION

To learn drawing or writing, a person first observes (encodes) the target image visually and uses a pen or a brush to scribble (decode), to reconstruct the original image. For an experienced painter, he or she foresees the consequences before taking any move, and could choose the optimal action.

Stroke-based image generation is fairly different from traditional image generation problems due to the intermediate rendering program. By traditional image generation methods, pixel values are directly calculated which allows effective optimization using back-propagation. While for stroke-based approaches, rather than learning to generate the image, it is more of learning to manipulate the painting program.

An intuitive yet potentially effective way to tackle the problem is to first learn this mapping from "stroke data" to the resulting image with a neural network, which is analogous to learning painting experience. An advantage of such a mapping over software is that it provides a continuous transformation. For any painting program, the pixel values of an image is calcuated based on the coordinate points along the trajectory of an action. Specific pixels are indexed by the discrete pixel coordinates, which cuts the gradient flow with respect to the action. In our implementation, the indexing is done by an MLP described in Section 3.

We further define "drawing" by giving a formal definition of "stroke". In our context, a "stroke" consists of color, brush radius, and a sequence of tuples containing the coordinate and pressure of each point along the trajectory. We will later describe this in detail in Section 3.

By doing so, we obtain a differentiable approximator of our painting software, which we call a "**generator**". We then tested the generator by training a vanilla CNN as an **agent** that encodes the image into "stroke" data as an input for the environment. Our proposed architecture, **StrokeNet**, basically comprises the two components, a **generator** and an **agent**.

Finally, the agent was trained to write and draw pictures of several popular datasets based on the generator. For the MNIST (LeCun & Cortes, 2010) digits, we evaluated the quality with a classifier trained solely on the original MNIST dataset, and tested the classifier on generated images. We explored the latent space of the agent as well.

[1] Code for the model at: `https://github.com/vexilligera/strokenet`.

2 RELATED WORK

Generative models such as VAEs(Kingma & Welling, 2013; Sohn et al., 2015) and GANs(Goodfellow et al., 2014; Mirza & Osindero, 2014; Radford et al., 2015; Arjovsky et al., 2017) have achieved huge success in image generation in recent years. These models generate images directly to pixel-level and thus could be trained through back-propagation effectively.

To mimic human drawing, attempts have been made to model the process of how humans learn to draw (Lake et al., 2015). Recent work generally falls into two categories: RNN-based approaches and reinforcement learning.

For RNN-based approaches such as SketchRNN (Ha & Eck, 2017) and handwriting generation with RNN by Graves (Graves, 2013), they both rely on sequential datasets. Thus for unpaired data, those models cannot be applied.

Another popular solution is to adopt reinforcement learning such as "artist agent"(Xie et al., 2012) and SPIRAL (Ganin et al., 2018). These methods train an agent that interact with the painting environment. For reinforcement learning tasks with large, continuous action space like this, the training process can be computationally costly and it could take the agent tens of epochs to converge.

To mitigate this situation, we simulate the environment in a differentiable manner much alike the idea in World Models (Ha & Schmidhuber, 2018) and earlier work done by J. Schmidhuber (Schmidhuber, 1990; 2018), where an agent learns from a neural network simulated, environment. In our scenario however, we face real-world learning problem and there are more subtleties in the design and training issues of the generator which we'll discuss in Section 3 and 4.

Differentiable rendering is an extensively researched topic in computer graphics. It's used to solve inverse rendering problems: given an image, how can we figure out the rendering process to recover the scene. Some differentiable renderers explicity model the relationship between the parameters and observations (Loper & Black, 2014), others use neural network to approximate the result (Nguyen-Phuoc et al., 2018) since neural nets are powerful function approximators. While little has been done on simulating 2D rendering process adopted in digital painting software, we used a generator neural network to meet our needs.

3 STROKENET ARCHITECTURE AND ENVIRONMENT

3.1 STROKE

We define a single stroke as follows,

$$s = \{(c, r), (x_1, y_1, p_1), \cdots, (x_n, y_n, p_n)\},\ n = 16, \tag{1}$$

where $c \in \mathbb{R}^3$ stands for RGB color, scalar r for brush radius, and tuple (x_i, y_i, p_i) for an anchor point on the stroke, consisting of x, y coordinate and pressure p, and n is the maximum number of points in a single stroke, in this case, 16. These values are normalized such that the coordinates corresponds to the default OpenGL coordinate system.

$$c_k, r, p_i \in [0, 1],\ x_i, y_i \in [-1, 1], \tag{2}$$

for $k = 1, 2, 3$ and $i = 1, 2, \cdots, n$. We used absolute coordinates for each point. It is notable that compared to the QuickDraw (Ha & Eck, 2017) dataset which contains longer lines, our strokes consist of much fewer points. We consider many trajectory points redundant since the stroke lines can be fitted by spline curves with fewer anchor points. For example, to fit a straight line, only two end-points are needed regardless of the length, in other words, stroke curves are usually scale-invariant. However, if we are to sample the data from a user input, we could have dozens of points along the trajectory. Hence we made the assumption of being able to represent curves with a few anchors. We later showed that a single stroke with only 16 anchors is able to fit most MNIST digits and generate twisted lines in Section 5. We further assumed that longer and more complicated lines can be decomposed into simple segments and extended our experiments to include recurrent drawing of multiple strokes to generate more complex drawings.

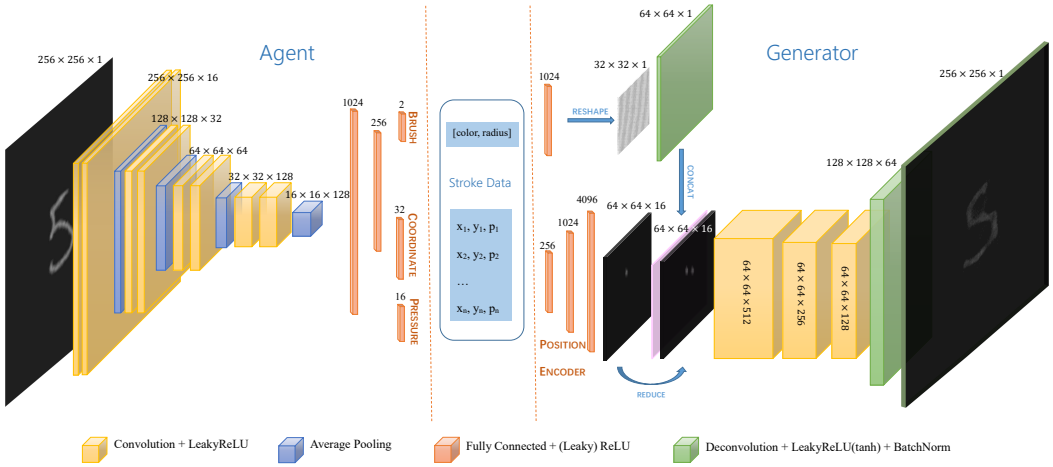

Figure 1: StrokeNet architecture. The generator part of the model outputs 256×256 images. The position encoder encodes input coordinate into 64×64 spatial feature for each point. The agent decodes different information about the stroke using three parallel FC-decoders.

3.2 Generator

The outline of the StrokeNet architecture is shown in Figure 1. The generator takes s as input, and projects the stroke data with two MLPs. One is the **position encoder** which encodes (x_i, y_i, p_i) into 64×64 feature maps, the other, **brush encoder** encodes the color and radius of the brush to a single 64×64 feature map. The color c' is a single gray scale scalar whose value equals to $\frac{1}{3}\sum_{k=1}^{3} c_k$, while color strokes are approximated by channel mixing described in Section 3.4. The features are then concatenated and passed to the (de)convolution layers.

To preserve the sequential and pressure information of each point (x_i, y_i, p_i), the **position encoder** first maps (x_i, y_i) to the corresponding position onto a 64×64 matrix by putting a bright dot on that point. This is modeled by a 2D Gaussian function with its peak scaled to 1, which simplifies to:

$$g_i(x, y) = \exp[-\frac{1}{2}((x - x_i)^2 + (y - y_i)^2)], \tag{3}$$

for $i = 1, 2, \cdots, n$ where the value is calculated for each point (x, y) on the 64×64 map. Denote this mapping from (x_i, y_i) to $\mathbb{R}^{64\times 64}$ as pos:

$$m_i = p_i \cdot pos(x_i, y_i),\ m_i \in \mathbb{R}^{64\times 64}. \tag{4}$$

By multiplying the corresponding pressure p_i, we now have n position features, in our setup, sixteen. This part of the generator is trained separately with random coordinates until it generates accurate and reliable signals.

However, if we directly feed these features into the (de)convolutional layers of the network, the generator fails partly due to the sparsity of the single brightness feature. Instead, we take every two neighbouring feature maps and add them together (denoted by "reduce" in Figure 1.),

$$f_i = m_i + m_{i+1},\ i = 1, 2, \cdots, n - 1. \tag{5}$$

Now, each feature map f_i represents a segment of the stroke. By learning to connect and curve the $n - 1$ "segments", we are able to reconstruct the stroke. By appending the encoded color and radius data we now have the feature with shape $64 \times 64 \times n$. We then feed the features into three (de)convolutional layers with batch-normalization (Ioffe & Szegedy, 2015) activated by LeakyReLU (Xu et al., 2015). The last layer is activated by tanh.

3.3 Agent

The agent is a VGG (Simonyan & Zisserman, 2014)-like CNN that encodes the target image into its underlying stroke representation s. Three parallel FC-decoders with different activations are

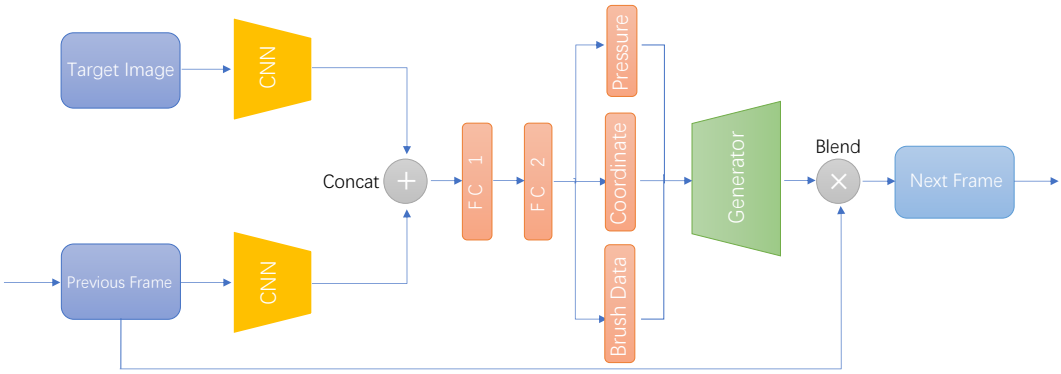

Figure 2: Recurrent version of StrokeNet. Two separate CNNs are used as encoders for the agent.

used to decode position (tanh), pressure (sigmoid) and brush data (sigmoid) from the feature. We used average-pooling instead of max-pooling to improve gradient flow. For the recurrent version of StrokeNet, two separate CNNs are trained for the target image and the drawing frame, as shown in Figure 2. In practice the target image feature is computed once for all steps.

3.4 Environment

We first built a painting software using JavaScript and WebGL. We later tailored this web application for our experiment. [2] The spline used to fit the anchor points is centripetal Catmull-Rom (Catmull & Rom, 1974; Barry & Goldman, 1988). A desirable feature about Catmull-Rom spline is that the curve goes through all control points, unlike the more commonly used Bezier curve (Sederberg & Farouki, 1992).

We then interpolate through the sampled points and draw circles around each center point as shown in Figure 3. For each pixel inside a circle, its color depends on various factors including attributes of the brush, blending algorithm, etc. Our generator is trained on the naive brush. When it comes to the color blending of two frames, the generator is fed with the mean value of input RGB color as a gray scale scalar, and its output is treated as an alpha map. Normalization and alpha-blending is then performed to yield the next color frame, to simulate real blending algorithm underlying the software. Denote the generator output at time-step t by $q^{(t)} \in \mathbb{R}^{256\times256}$, the frame image by $r^{(t)} \in \mathbb{R}^{3\times256\times256}$, RGB color of the brush by $c \in \mathbb{R}^3$, the blending process is approximated as follows,

$$n^{(t)} = \frac{q^{(t)}}{\max\limits_{1\le i,j\le 256} q_{ij}^{(t)}}, \tag{6}$$

$$r_k^{(t)} = (J - n^{(t)}) r_k^{(t-1)} + c_k n^{(t)} \tag{7}$$

for $k = 1, 2, 3$ corresponding to the RGB channels, where J denotes a 256×256 all-one matrix.

4 Training Methods

4.1 Dataset for Generator

For the generator, a dataset containing different kinds of human scribbles within a single stroke would be an ideal candidate for training, which sadly doesn't exist. We need to generate a large amount of samples each of length n that captures both the randomness and the smoothness of human writing. Pure random walk results in wiggling strokes which is ugly and hard to fit, while polynomials offer too little variation in shapes. Thus it is natural to incorporate **chaos**, most notably, the motion of three-body (Nielsen et al., 2001).

[2] Code for the web application available at: `https://github.com/vexilligera/drawwebapp`.

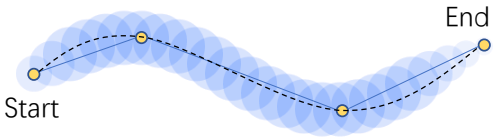

Figure 3: Illustration of how a stroke is rendered.

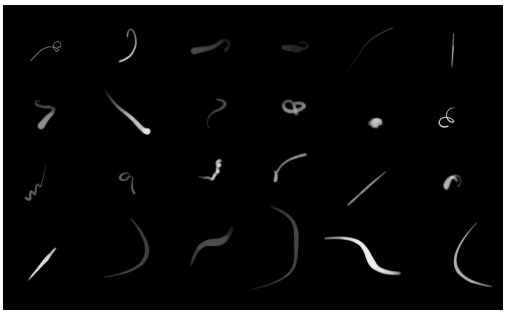

Figure 4: Images from our three-body dataset.

There's no closed-form solution to three-body problem, and error accumulates in simulation using numerical methods, leading to unpredictable and chaotic results. We simulate three-body motion in space (z-component for pressure) with random initial conditions and sample the trajectories as strokes for our dataset. The simulation is done with a set of equations using Newton's universal law of gravitation:

$$\begin{cases} \vec{F_1} = \frac{Gm_1m_2}{\|P_2-P_1\|_2^3}(P_2-P_1) + \frac{Gm_1m_3}{\|P_3-P_1\|_2^3}(P_3-P_1) \\ \vec{F_2} = \frac{Gm_1m_2}{\|P_1-P_2\|_2^3}(P_1-P_2) + \frac{Gm_2m_3}{\|P_3-P_2\|_2^3}(P_3-P_2) \\ \vec{F_3} = \frac{Gm_1m_3}{\|P_1-P_3\|_2^3}(P_1-P_3) + \frac{Gm_2m_3}{\|P_2-P_3\|_2^3}(P_2-P_3) \end{cases}, \tag{8}$$

where $P_i (i = 1, 2, 3,\ P_i \in \mathbb{R}^3)$ denotes the position of the three objects respectively, $\vec{F_i}$ denotes the gravitational force exerted on the ith object. In our simulation we set mass $m_1 = m_2 = m_3 = 1$ and gravitational constant $G = 5 \times 10^{-5}$. We also always keep our camera (origin point) at the center of the triangle formed by the three objects to maintain relatively stable "footage".

Using this method we collected about 600K images since there's virtually no cost to generate samples. Samples from the dataset are shown in Figure 4.

4.2 Datasets for Agent

To prove the effectivess of our neural environment, we trained an agent to perform drawing task on several popular datasets, from characters to drawings, with the generator part frozen. For MNIST and Omniglot, we trained an agent to draw the characters within one stroke. We later trained the recurrent StrokeNet on more complex datasets like QuickDraw and KanjiVG (Ofusa et al., 2017). We resized all the input images to 256×256 with anti-alias and paddings.

4.3 Training Methodology

Intially we train the **position encoder** guided by function pos that maps a coordinate to a 64×64 matrix with l^2 distance to measure the loss. Next we **freeze** the **position encoder** and train the other parts of the generator, again with l^2 loss to measure the performance on the three-body dataset. It can be found that smaller batch size results in more accurate images. We trained the generator with a batch size of 64 until the loss no longer improves. We then set the batch size to 32 to sharpen the neural network.

To train the **agent**, we freeze the **generator**. Denote the agent loss as l_{agent}, the generated image and ground-truth image as i_{gen} and i_{gt} respectively, the loss is defined as:

$$l_{agent} = \|i_{gen} - i_{gt}\|_2^2 + \frac{\lambda}{n-1}\sum_{k=1}^{n-1}\|P_k - P_{k+1}\|_2^2, \tag{9}$$

where $P_k = [x_k, y_k, p_k]^T$ is the data describing the kth anchor point on the stroke. Here the summation term constrains the average distance between neighbouring points, where λ denotes the penalty strength. If we drop this term, the agent fails to learn the correct order of the points in a stroke because the generator itself is, after all, not robust to all cases of input, and is very likely to produce wrong results for sequences with large gaps between neighbouring points.

5 EXPERIMENTS

All experiments are conducted on a single NVIDIA Tesla P40 GPU. We first experimented with single step StrokeNet on MNIST and Omniglot, then we experimented recurrent StrokeNet with QuickDraw and Kanji. For the MNIST dataset, we later enforced a Gaussian prior to the latent variable and explored the latent space of the agent by linear interpolation. Finally, for a quantitative evaluation of the model, we trained a classifier on MNIST, and tested the classifier with images generated by the agent. The close accuracies indicate the quality of the generated images.

5.1 SINGLE-STEP STROKENET

It can be seen that a single stroke provides rich expressive power for different shapes. The generator generalizes well to unseen stroke patterns other than the synthesized three-body dataset. On the Omniglot dataset, since many characters consist of multiple strokes while the agent can only draw one, the agent tries to capture the contour of the character.

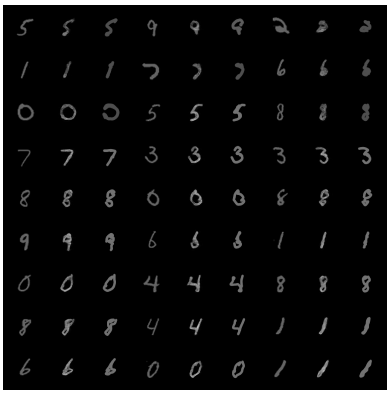

Figure 5: Agent trained on MNIST. MNIST sample (left), generator output (middle), WebApp reconstruction (right). 1.5 epochs.

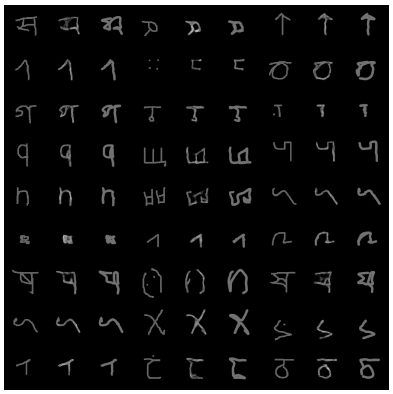

Figure 6: Agent trained on Omniglot dataset learns to "sketch" the characters. Layout is the same as Figure 5. 10^4 iterations.

5.2 RECURRENT-STEP STROKENET

For more complex datasets, multiple steps of strokes are needed. Again the agent does pretty well to capture the contour of the given image. However, it seems that the agent has trouble to recover the details of the pictures, and tends to smear inside the boundaries with thick strokes.

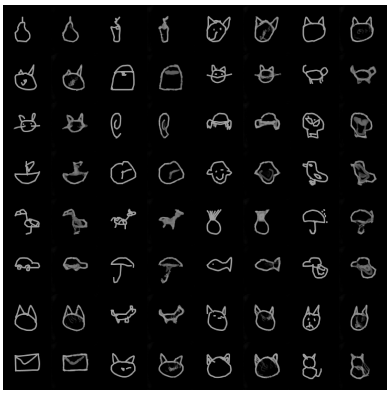

Figure 7: Agent trained on QuickDraw. Sample (left), reconstruction (right). 6 recurrent steps. 300K-image subset, 5 epochs, 10^5 iterations.

Figure 8: Agent trained on KanjiVG dataset. Evaluated on a test-set of simple characters. 10^5 iterations. 8 recurrent steps.

Figure 9: Latent space interpolation. Leftmost and rightmost columns are images from MNIST dataset. Middles are the rendered images with interpolation factors varying from 0 to 1.

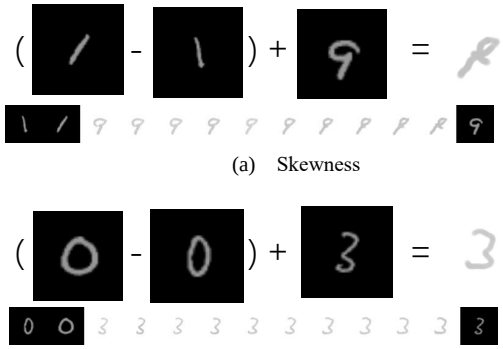

Figure 10: Latent space arithmetics. (a) and (b) demonstrate different attributes of the digits.

5.3 Latent Space Exploration

To convert the agent into a latent space generative model, we experimented with the VAE version of the agent, where the feature obtained from the last layer of CNN is projected into two vectors representing the means μ and standard deviations (activated by softplus) σ, both of 1024 dimensions. A vector noise of i.i.d. Gaussian $U \sim N(0, I)$ is sampled, latent variable z is given by

$$z = \mu + \sigma \odot U. \tag{10}$$

We did latent space interpolation with the agent trained on MNIST. The simple data led to easily interpretable results. Since the images are generated by strokes, the digits transform smoothly to one another. That is to say, the results looked as if we were directly interpolating the stroke data. Results are shown in Figure 9 and 10.

5.4 Performance Evaluation

In order to evaluate the agent, we trained a 5-layer CNN classifier solely on pre-processed MNIST dataset, which is also the input to the MNIST agent. The size of the image is 256×256, so there is some performance drop to the classification task compared to traditional 28×28 images. The classifier is then used to evaluate the paired test-set image generated by the agent. The accuracies reflect the quality of the generated images.

Table 1: MNIST Classification accuracy

TEST DATA	ACCURACY
Pre-processed MNIST images	90.82%
MNIST Agent Output (3 steps)	88.43%
MNIST Agent Output (1 step)	79.33%
MNIST Agent Output (1 step, VAE)	67.21%

6 Discussion

For future work, there're several major improvements we want to make both to the network structure and to the algorithm.

The recurrent structure adopted here is of the simplest form. We use this setup because we consider drawing as a Markov process, where the current action only depends on what the agent sees, the target image and the previous frame. More advanced structures like LSTM (Hochreiter & Schmidhuber, 1997) or GRU (Chung et al., 2014) may boost the performance. For the agent,

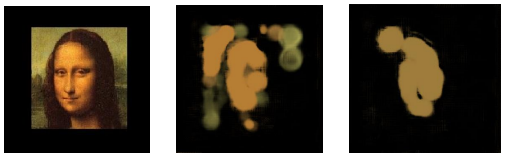

(a) (b) (c)

Figure 11: 16-step color image reconstruction. (a) Mona Lisa. (b) Successful reconstruction includes use of different colors. (c) Fail to use different colors.

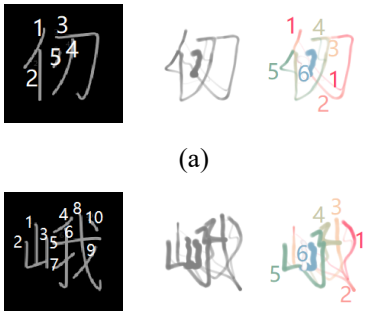

(a)

(b)

Figure 12: Comparison of stroke orders between human and agent. We can see the stroke order is completely chaotic compared to natural order.

various attention mechanism could be incorporated to help the agent focus on undrawn regions, so that smear and blurry scribbles might be prevented.

Secondly, The generator and the agent were trained as two separate parts throughout the experiment. We can somehow train them as a whole: during the training of the agent, store all the intermediate stroke data. After a period of training, sample images from the real environment with the stroke data just collected, and train the generator with the data. By doing so in an iterative manner, the network could be more aware of what it's exactly doing, while the changing generator may potentially provide more valuable overall gradients.

It's also found useful to add a bit of randomness to the learning rate. Since different decoders of the agent learn at different rates, stocasticity results in more appealing results. For example, the agent usually fails to generalize to color images because it always sticks with one global average color (as shown in Figure 11). However, it sometimes generates appealing results with some randomness added during the training. Also, the agent avoids to make intersecting strokes over all datasets, although such actions are harmless and should be totally encouraged and explored! Thus, random sampling techniques could be added to the decision making process to encourage bolder moves.

Finally, for the evaluation metrics, the naive l^2 loss can be combined with discriminator loss given its popularity and mightiness to achieve adversarial learning.

7 Conclusion

In this paper we bring a proof-of-concept that an agent is able to learn from its neural simulation of an environment. Especially when the environment is definite given the action, or contains a huge action space which requires massive computation, the proposed approach could be useful. Our primary contribution is that we devised a model-based method to approximate non-differentiable environment with neural network, and the agent trained with our method converges quickly on several datasets. It is able to adapt its skills to real world. Hopefully such approaches can be useful when dealing with more difficult reinforcement learning problems.

REFERENCES

Martin Arjovsky, Soumith Chintala, and Léon Bottou. Wasserstein generative adversarial networks. In Doina Precup and Yee Whye Teh (eds.), *Proceedings of the 34th International Conference on Machine Learning*, volume 70 of *Proceedings of Machine Learning Research*, pp. 214–223, International Convention Centre, Sydney, Australia, 06–11 Aug 2017. PMLR.

Phillip J. Barry and Ronald N. Goldman. A recursive evaluation algorithm for a class of catmull-rom splines. *SIGGRAPH Comput. Graph.*, 22(4):199–204, June 1988. ISSN 0097-8930. doi: 10.1145/378456.378511.

Edwin Catmull and Raphael Rom. A class of local interpolating splines. *Computer Aided Geometric Design*, pp. 317–326, 1974.

Junyoung Chung, Çaglar Gülçehre, KyungHyun Cho, and Yoshua Bengio. Empirical evaluation of gated recurrent neural networks on sequence modeling. *CoRR*, abs/1412.3555, 2014.

Yaroslav Ganin, Tejas Kulkarni, Igor Babuschkin, S. M. Ali Eslami, and Oriol Vinyals. Synthesizing programs for images using reinforced adversarial learning. *CoRR*, abs/1804.01118, 2018.

Ian Goodfellow, Jean Pouget-Abadie, Mehdi Mirza, Bing Xu, David Warde-Farley, Sherjil Ozair, Aaron Courville, and Yoshua Bengio. Generative adversarial nets. In Z. Ghahramani, M. Welling, C. Cortes, N. D. Lawrence, and K. Q. Weinberger (eds.), *Advances in Neural Information Processing Systems 27*, pp. 2672–2680. Curran Associates, Inc., 2014.

Alex Graves. Generating sequences with recurrent neural networks. *CoRR*, abs/1308.0850, 2013.

David Ha and Douglas Eck. A neural representation of sketch drawings. *CoRR*, abs/1704.03477, 2017.

David Ha and Jürgen Schmidhuber. World models. *CoRR*, abs/1803.10122, 2018.

Sepp Hochreiter and Jürgen Schmidhuber. Long short-term memory. *Neural computation*, 9(8): 1735–1780, 1997.

Sergey Ioffe and Christian Szegedy. Batch normalization: Accelerating deep network training by reducing internal covariate shift. *CoRR*, abs/1502.03167, 2015.

Diederik P. Kingma and Max Welling. Auto-encoding variational bayes. *CoRR*, abs/1312.6114, 2013.

Brenden M. Lake, Ruslan Salakhutdinov, and Joshua B. Tenenbaum. Human-level concept learning through probabilistic program induction. *Science*, 2015.

Yann LeCun and Corinna Cortes. MNIST handwritten digit database. 2010.

Matthew M. Loper and Michael J. Black. OpenDR: An approximate differentiable renderer. In *Computer Vision – ECCV 2014*, volume 8695 of *Lecture Notes in Computer Science*, pp. 154–169. Springer International Publishing, September 2014.

Mehdi Mirza and Simon Osindero. Conditional generative adversarial nets. *CoRR*, abs/1411.1784, 2014.

Thu Nguyen-Phuoc, Chuan Li, Stephen Balaban, and Yong-Liang Yang. Rendernet: A deep convolutional network for differentiable rendering from 3d shapes. *arXiv preprint arXiv*, abs/1806.06575, 2018.

E. Nielsen, D.V. Fedorov, A.S. Jensen, and E. Garrido. The three-body problem with short-range interactions. *Physics Reports*, 347(5):373 – 459, 2001. ISSN 0370-1573. doi: https://doi.org/10.1016/S0370-1573(00)00107-1.

Kenichiro Ofusa, Tomo Miyazaki, Yoshihiro Sugaya, and Shinichiro Omachi. Glyph-based data augmentation for accurate kanji character recognition. In *14th IAPR International Conference on Document Analysis and Recognition, ICDAR 2017, Kyoto, Japan, November 9-15, 2017*, pp. 597–602. IEEE, 2017. ISBN 978-1-5386-3586-5. doi: https://doi.org/10.1109/ICDAR.2017.103.

Alec Radford, Luke Metz, and Soumith Chintala. Unsupervised representation learning with deep convolutional generative adversarial networks. *CoRR*, abs/1511.06434, 2015.

Jürgen Schmidhuber. Making the world differentiable: On using self-supervised fully recurrent neural networks for dynamic reinforcement learning and planning in non-stationary environments. Technical report, 1990.

Jürgen Schmidhuber. One big net for everything. *CoRR*, abs/1802.08864, 2018.

Thomas W. Sederberg and Rida T. Farouki. Approximation by interval bezier curves. *IEEE Computer Graphics and Applications*, 12(5):87–95, 1992. doi: http://doi.ieeecomputersociety.org/10.1109/38.156018.

Karen Simonyan and Andrew Zisserman. Very deep convolutional networks for large-scale image recognition. *CoRR*, abs/1409.1556, 2014.

Kihyuk Sohn, Honglak Lee, and Xinchen Yan. Learning structured output representation using deep conditional generative models. In C. Cortes, N. D. Lawrence, D. D. Lee, M. Sugiyama, and R. Garnett (eds.), *Advances in Neural Information Processing Systems 28*, pp. 3483–3491. Curran Associates, Inc., 2015.

Ning Xie, Hirotaka Hachiya, and Masashi Sugiyama. Artist agent: A reinforcement learning approach to automatic stroke generation in oriental ink painting. *CoRR*, abs/1206.4634, 2012.

Bing Xu, Naiyan Wang, Tianqi Chen, and Mu Li. Empirical evaluation of rectified activations in convolutional network. *CoRR*, abs/1505.00853, 2015.

8 APPENDIX

8.1 ENVIRONMENT DETAILS

Let $P_i = [x_i, y_i]^T$ denote the coordinate of a sampled point. For a curve defined by points P_0, P_1, P_2, P_3, the spline can be produced by:

$$C = \frac{t_2 - t}{t_2 - t_1} B_1 + \frac{t - t_1}{t_2 - t_1} B_2, \tag{11}$$

where

$$\begin{aligned} B_1 &= \frac{t_2 - t}{t_2 - t_0} A_1 + \frac{t - t_0}{t_2 - t_0} A_2, \quad B_2 = \frac{t_3 - t}{t_3 - t_1} A_2 + \frac{t - t_1}{t_3 - t_1} A_3, \\ A_1 &= \frac{t_1 - t}{t_1 - t_0} P_0 + \frac{t - t_0}{t_1 - t_0} P_1, \quad A_2 = \frac{t_2 - t}{t_2 - t_1} P_1 + \frac{t - t_1}{t_2 - t_1} P_2, \\ A_3 &= \frac{t_3 - t}{t_3 - t_2} P_2 + \frac{t - t_2}{t_3 - t_2} P_3, \quad t_{i+1} = \|P_{i+1} - Pi\|_2^{\alpha} + t_i. \end{aligned} \tag{12}$$

with $\alpha = 0.5$, $t_0 = 0$ and $i = 0, 1, 2, 3$

By interpolating t from t_1 to t_2 linearly, we generate the curve between P_1 and P_2. The pressure values between neighbouring points are interpolated linearly.

8.2 LOSSES

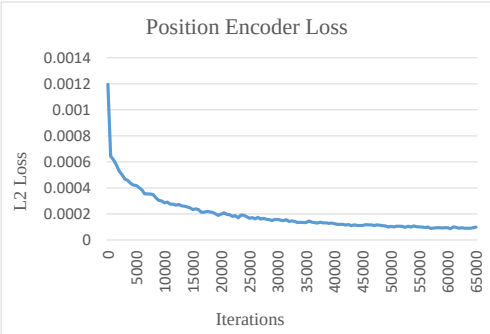

(a) Loss of encoder when trained separately at first.

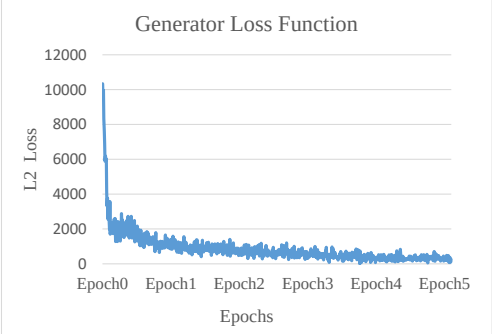

(b) Loss of generator trained on our 600K dataset.

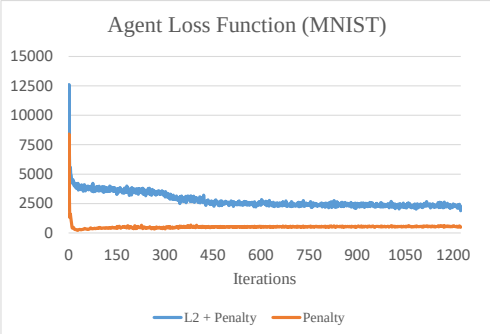

(c) Agent trained on MNIST, $\lambda = 200$.

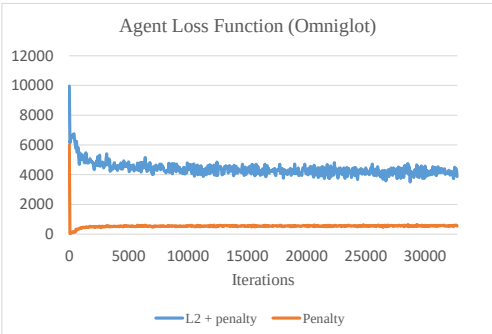

(d) Agent trained on Omniglot, $\lambda = 200$.

Figure 13: Training loss of generator and agent. The agent loss equals to the l^2 distance between the generator output and agent input plus the penalty term constraining the average point distance within a stroke. For (c) and (d) the learning rate is set to 10^{-4}, batch size equals to 64.

8.3 MISCELLANEOUS RESULTS

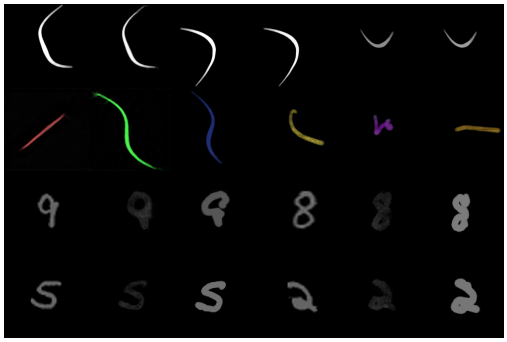

Figure 14: A trained StrokeNet generates images that resemble the output of painting software. The first row depicts results generated by our model (left) and by the software (right) given the same input. The second row shows the model could produce strokes with color and texture using simple arithmetic operations. The third and fourth row shows the model's ability to draw MNIST digits (left) on both its own generative model (middle) and real-world painting software (right).

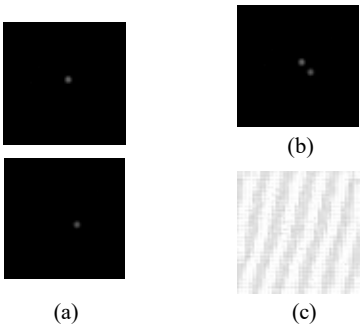

Figure 15: (a) A trained position encoder maps two (x_i, y_i, p_i) tuples to two feature maps. (b) Each pair of neighbouring features are added together to eliminate sparsity and preserve sequential information. (c) A trained brush encoder encodes color and radius information into a spatial feature which is later concatenated to the end of position features.

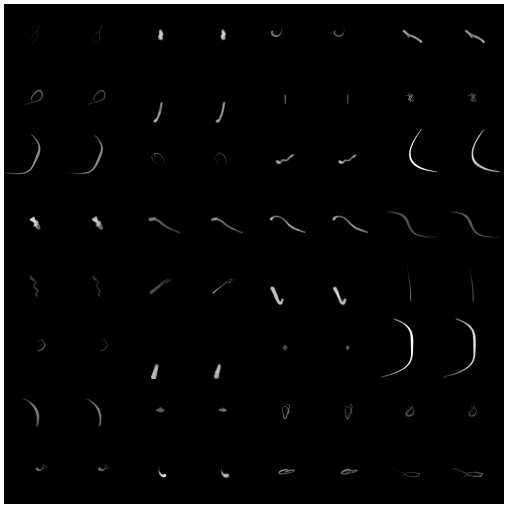

Figure 16: The generator tries to predict what the real environment would ouput given the same input stroke data. Software output (left), generator prediction (right).

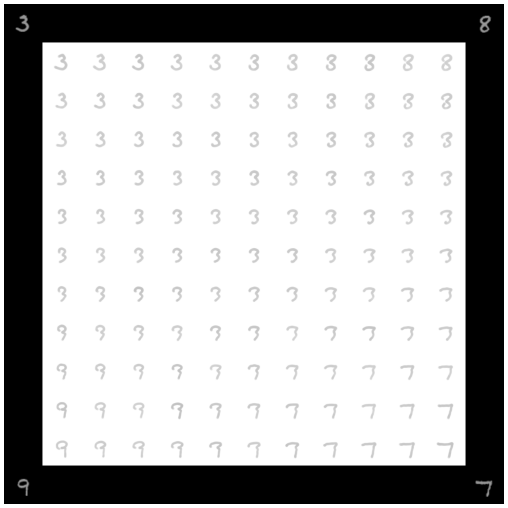

Figure 17: Interpolation across four digits. In the corners are the four MNIST samples.